Influence of tip speed ratio on a real wind turbine wake profile using LiDAR

Satoshi Nakashima*, Hiroaki Fujio, Nobutoshi Nishio, Chuichi Arakawa, Makoto Iida**

Satoshi Nakashima, Hiroaki Fujio, Chuichi Arakawa and Makoto Iida
The University of Tokyo, 7-3-1 Hongo, Bunkyo-ku, Tokyo, Japan
Nobutoshi Nishio
Electric Power Development Co., Ltd., 6-15-1 Ginza, Chuoku-ku, Tokyo, Japan

Key Words: Wind Turbine, Wake, Field Test, LiDAR, Tip speed ratio

Abstract

When a wind turbine operates in the wake of an upstream turbine, it produces less power than it would in a freestream. To determine the appropriate turbine-setting distance, understanding the characteristics of a wind turbine wake is important. Various studies have been conducted for comprehending wake characteristics. For example, wind tunnel tests showed the influence of tip speed ratio (defined as the tip speed divided by the inflow speed) on wind turbine wake. Remote sensing devices such as Light Detection and Ranging (LiDAR) are used for field measurements of the wake produced by real wind turbines. However, few studies exist that focus on the influence of tip speed ratio on a real turbine wake. In this study, we investigated the effects of tip speed ratio on actual-scale wind turbine wake characteristics by measuring the wake of a real wind turbine on flat terrain using LiDAR. For the wake measurement, we use a LiDAR that can perform two-dimensional vertical scans of the wind field, and the vertical profiles of the mean wind speed were calculated from the average wind speed in three different tip speed ratio range. Downstream recovery of the velocity deficit is more rapid at lower tip speed ratio, and this trend is dissimilar to the results of the previous wind tunnel test. Furthermore, the twin-shape of the profile brakes more slowly at higher tip speed ratio. Moreover, the wind speed outside of the rotor range is accelerated in the near-wake.

1. Introduction

Wind turbines arranged in a wind farm are an efficient form of wind turbine operation from a profitability viewpoint; however, when a wind turbine operates in the wake of an upstream turbine, it produces less power than it does in a freestream. The properties of a wind turbine wake depend on many factors such as wind conditions, wind turbine operating conditions and yaw angle [1]–[3]. Previous studies of wind tunnel tests showed that the turbulence intensity in the freestream affects the downstream recovery of the velocity deficit in the wake [4], and a field test found that the velocity deficit in the wake recovers more rapidly in a field than in a wind tunnel [5]. Some research studies reported the influences of tip speed ratio (defined as the tip speed divided by the inflow speed) and yaw angle on wind turbine wake [3], [6], [7]. In these wind tunnel tests, hot-wire anemometer, pitot-static probe, Laser Doppler Anemometer and particle image velocimetry were used for the wake measurements; however, these devices are not available for some MW-turbine-scale wake measurements. In addition, common measurements for actual-turbine-scale using sonic anemometers and cup anemometers set up on a turbine nacelle or a met mast are point observation devices and are not suitable for actual-scale wake measurements.

Light Detection and Ranging (LiDAR) is one of the devices used for field measurements of the wake produced by real wind turbines. LiDAR can measure wind flows over a wide range and at high altitude with high resolution. Gallacher and More used LiDAR to measure the wake of a wind turbine in order to investigate the wake decay length, and they compared the PARK wake model with the measured data using LiDAR to assess its effectiveness in wake modelling [8]. Another set of field measurements of wake using two LiDARs was performed by Iungo et al.; their study showed that the mean vertical velocity is practically negligible for all the considered downstream locations [9].

In order to settle the appropriate turbine-setting distance, wake models that assess interactions between turbines are required; however, there is currently no general-purpose wake model. Therefore,

*Presenting author. **Corresponding author.
E-mail:
nakashima.satoshi@gg.cfdl.t.u-tokyo.ac.jp (Satoshi Nakashima)
iida@ilab.eco.rcast.u-tokyo.ac.jp (Makoto Iida)

data storage of field measurements is necessary for the development of general-purpose wake model of real turbines. Especially in Japan, it is important to investigate the effects of terrain configuration, with a high turbulence intensity found in complex terrains and mountainous terrains. It is also important to study the influences of the wind turbine operation conditions on the wake characteristics of real turbines.

The aim of this paper is to store the data obtained from field tests for the development of real-scale wake models that include the influences of the operation of wind turbines on the wake by investigating the effects of tip speed ratio on the real-scale wake characteristics via measurements of the wake of a real wind turbine at a flat terrain using LiDAR.

2. Field Test

2-1. Test site and experimental setup

The LiDAR field test was performed at a flat terrain site in Japan; Figure 1 shows the general view of the field test site. The wind turbine was located near the shore line.

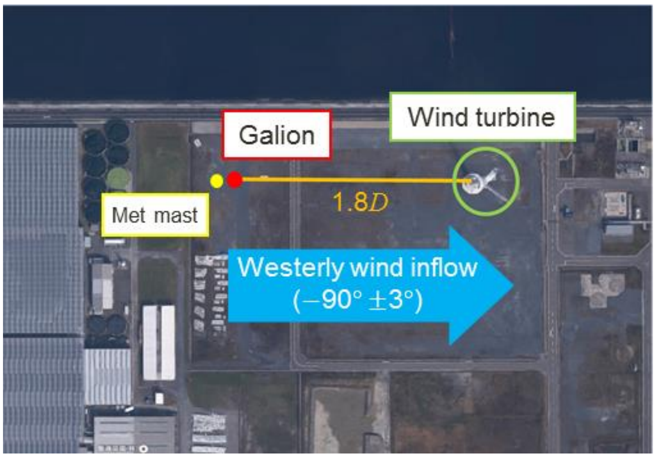

Figure 1: Overview of the field test site (D: rotor diameter).

Table 1 shows the major specifications for the wind turbine. Sonic anemometers and wind vanes were set up on the turbine nacelle.

Table 1: Wind turbine specifications

Rated power	2,700 kW
Rotor diameter	103.4 m
Hub height	82.5 m
Rated Wind Speed	13 m/s
Cut-in wind speed	4.0 m/s
Type	Horizontal axis (upwind)

The Galion LiDAR, developed by SgurrEnergy, was used for the measurements (see Figure 2). Using this LiDAR, two-dimensional vertical scans of the wind field were performed by varying the elevation angle of the laser while holding the azimuth angle constant (RHI scans). The major specifications for the Galion system are shown in Table 2.

Figure 2: Galion LiDAR

Table 2: Galion LiDAR system specifications

Measurement range	75–1005 m
Spatial resolution	30 m
Accuracy	0.1 m/s
Wind speed range	0–70 m/s
Sampling time between two scans	3.4 s
Laser elevation angles	3°–75° 3° intervals

In this study, the azimuth angle of the laser was fixed at 90° (east of the Galion, 0° is the north). By setting the azimuth angle on the direction of the center of the turbine, two-dimensional measurements using the LiDAR were conducted over the vertical symmetry plane of the wind turbine wake. The Galion was located 1.8D west from the wind turbine (see Figure 1). The test was performed with 25 different laser elevation angles evenly spaced by 3°. Each vertical scan required approximately 85 s.

The horizontal wind speed was calculated from Equation 1 by assuming the negligible vertical wind speed and the wind direction from the supervisory control and data acquisition (SCADA) data. Schematics of measurement of wind speed using Galion is shown in Figure 3. Here, U is horizontal wind speed, W is vertical wind speed (assuming W = 0), θ_{wind} is wind direction (assuming wind direction from the SCADA), θ_{scan} is azimuth angle of the laser (fixed at 90°), U_{scan} is laser azimuthal component of horizontal wind speed, α is elevation angle of the laser, and V_r is component of velocity in the line of sight.

$$V_r = -U\cos\alpha\cos(\theta_{scan} - \theta_{wind}) + W\sin\alpha \quad (1)$$

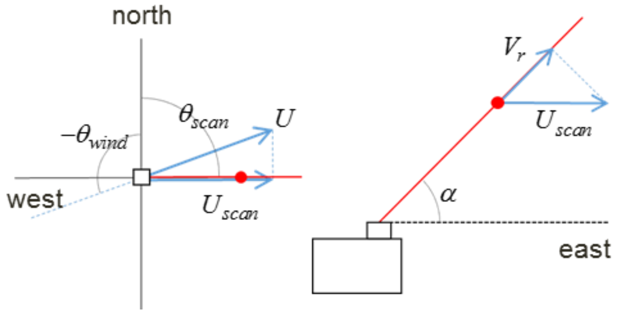

Figure 3: Schematics of measurement of wind speed using Galion (left: top view, and right: side view).

2-2. NTF transform of nacelle wind speed

The wind measured by the anemometers on the nacelle of the tested wind turbine is potentially inferenced by the nacelle structure (see Figure 4). In this case, it is recommended transforming nacelle wind speed by using Nacelle Transfer Function (NTF) [10]. NTF is defined by Equation 2. $u_{nacelle,i}$ is the mean nacelle wind speed in bin i. $u_{free,i}$ is the mean met mast wind speed in bin i. $u_{nacelle}$ is the wind speed measured by the nacelle anemometer. $u_{estimated}$ is the estimated wind speed based on the nacelle wind speed and the mast wind speed.

$$u_{estimated} = \frac{u_{free,i+1} - u_{free,i}}{u_{\text{nacelle},i+1} - u_{\text{nacelle},i}} \times \left(u_{\text{nacelle}} - u_{\text{nacelle},i}\right) + u_{free,i} \quad (2)$$

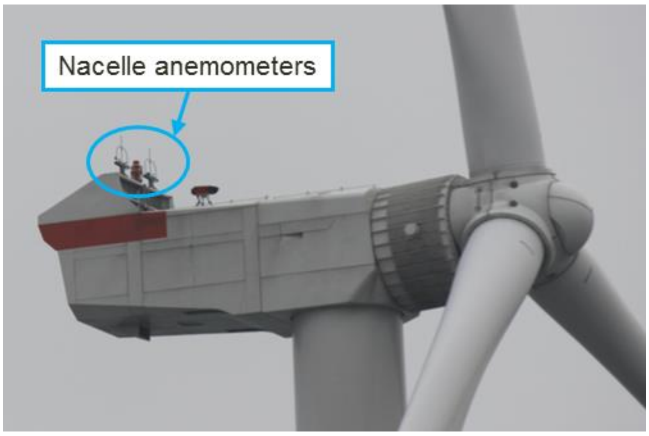

Figure 4: Installation status of nacelle anemometers

2-3. Wind condition on the field test site

The SCADA data of the tested wind turbine for the testing period include the wind speed at hub height from an anemometer mounted on the nacelle, the nacelle yaw angle, the rotational speed of the wind turbine rotor, and the generated power. The nacelle wind speed is transformed by using NTF, and the transformed wind speed is denoted as NTF wind speed. A histogram of the mean NTF wind speed obtained is shown in Figure 5. The figure shows that wind speeds between 2 and 7 m/s were the primary speeds in the test site during the testing period. A wind rose evaluated using the SCADA data is shown in Figure 6. The figure shows that major wind directions during the testing period were ESE and SW. The relationship between the power coefficient C_P and tip speed ratio λ is shown in Figure 7. A histogram of the mean tip speed ratio obtained from the NTF data is shown in Figure 8. C_P is defined by Equation 3 and λ is defined by Equation 4. P is the generated power, ρ is the air density, R is rotor radius, U_∞ is nacelle wind speed, and Ω is the angular velocity of the blade rotation respectively.

The vertical profiles of the mean westerly wind speed were calculated from the average wind speed in each tip speed ratio (*TSR*, λ) range (A), (B), and (C) in Figure 7 and Figure 8.

$$C_P = \frac{P}{\frac{1}{2}\rho U_\infty^3 \pi R^2} \quad (3)$$

$$\lambda = \frac{R\Omega}{U_\infty} \quad (4)$$

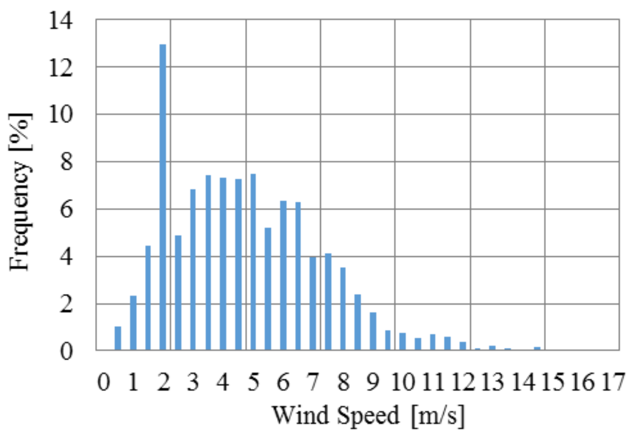

Figure 5: Histogram of the mean wind speed obtained from NTF data during the testing period with a sampling time of 10 min.

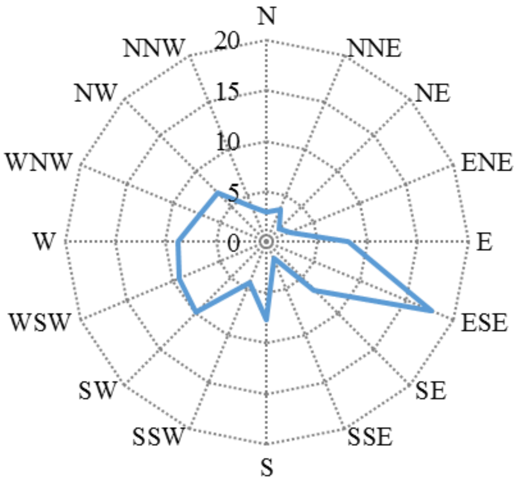

Figure 6: Wind rose evaluated using the SCADA data during the testing period.

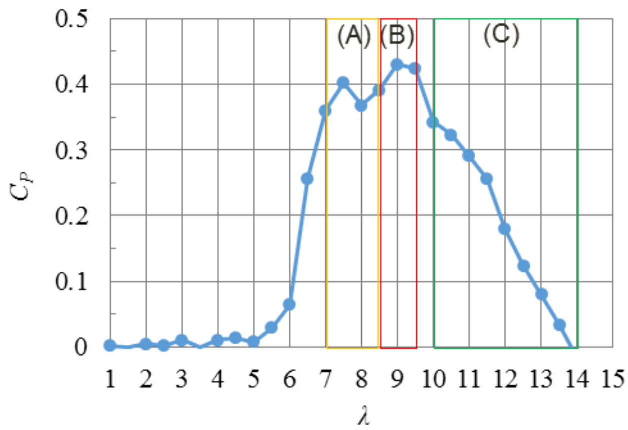

Figure 7: Power coefficient (C_P) versus tip speed ratio (λ) evaluated from the NTF data for the testing period: (A) optimum performance region (lower *TSR*, λ = 7 – 8.5), (B) optimum performance region (higher *TSR*, λ = 8.5 – 9.5), (C) high *TSR* region (λ = 10 – 14).

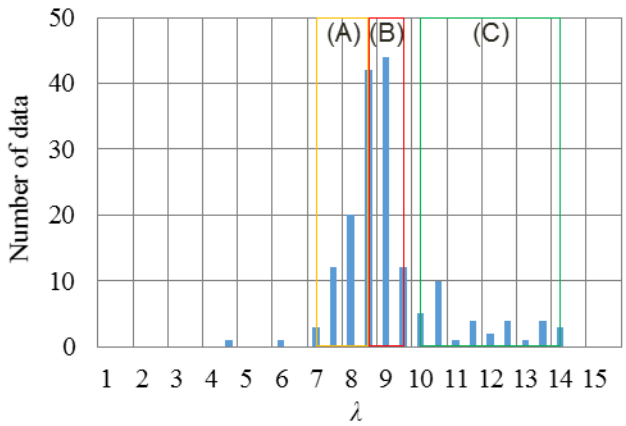

Figure 8: Number of data versus λ in the westerly wind condition (90° ± 3°).

3. Experimental results

The positions of the vertical profiles obtained using the LiDAR are shown in Figure 9, where D is the rotor diameter.

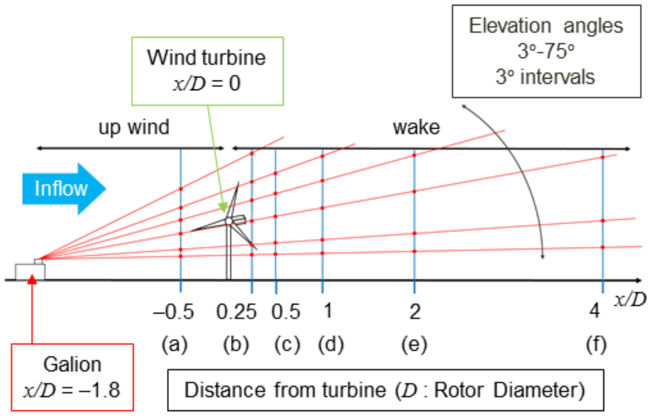

Figure 9: Positions of vertical profiles obtained by RHI scans using the Galion.

The vertical profiles of the mean westerly wind speed in the *TSR* regions (A), (B), (C) are shown in Figure 10. H is the hub height. The red lines in Figure 10 indicate the range of the wind turbine rotor. The wind speed at the positions (b) – (f) is normalized with U_{inflow}, the inflow horizontal wind speed at the position (a). The error bars show the mean ± one standard deviation.

Downstream recovery of the velocity deficit is more rapid at lower tip speed ratio, as shown in Figure 10 (e) and (f). In the region (A), the wake deficit has almost recovered at $4D$ from the wind turbine, while the wake deficit remains at $4D$ in the regions (B) and (C). This trend is dissimilar to the results of the previous wind tunnel test [7]. However, note that the shapes of the near wake profiles are different between this field test (Figure 10 (b) and (c)) and the wind tunnel test.

The twin-mountain shape of the profile brakes more slowly at higher tip speed ratio, as shown in Figure 10 (b) – (d). In the region (A), the twin-mountain shape has broken at $1D$ from the wind turbine, while the shape remains at $1D$ in the regions (B) and (C). The radial velocity may act as a barrier that prevents the wake from mixing with the main stream, and the influence of the radial velocity is stronger at higher tip speed ratio.

The wind speed outside of the rotor range (at lower height, $(z\text{-}H)/D$ = −0.75 ~ 0.5) is accelerated in the near-wake, as shown in Figure 10 (b) – (d), especially in high *TSR* region (C).

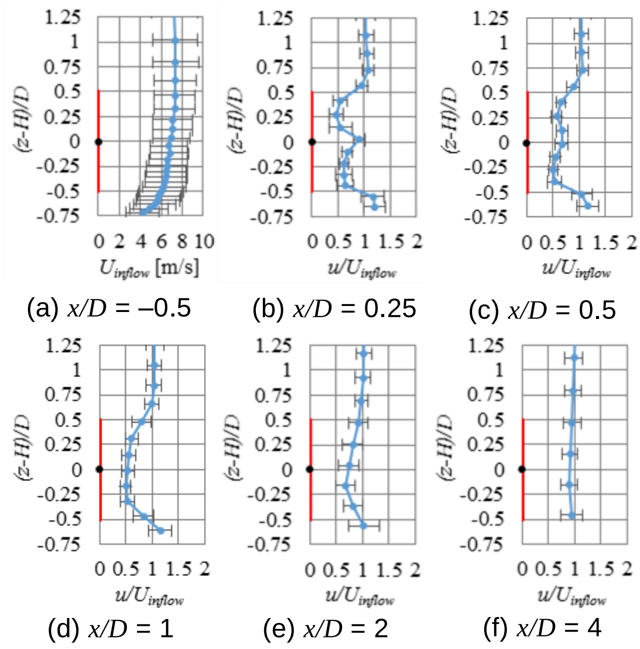

The *TSR* region (A): λ = 7 – 8.5

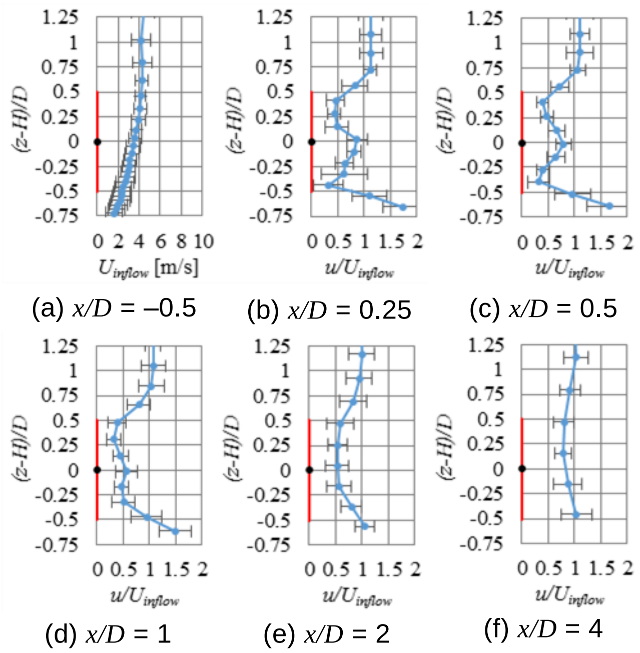

The *TSR* region (C): λ = 10 – 14

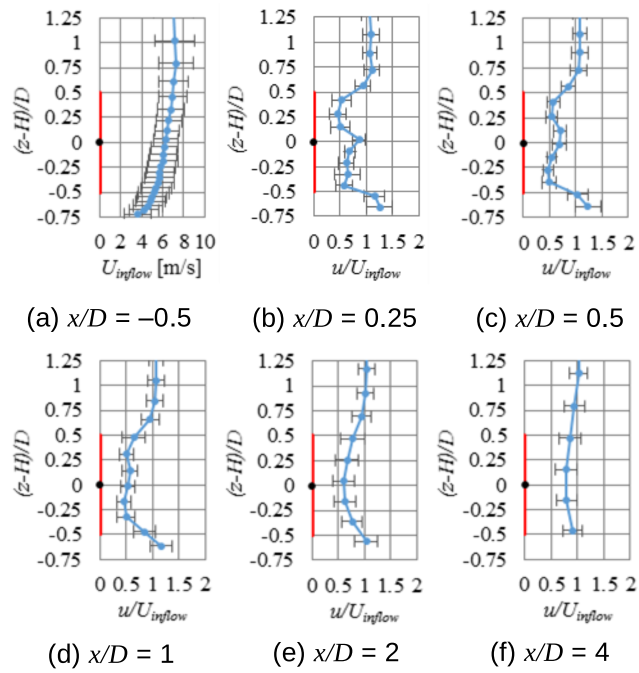

The *TSR* region (B): λ = 8.5 – 9.5

Figure 10: Vertical profiles of the mean horizontal wind speed. Downwind distance from the turbine (a) –0.5D (b) 0.25D (c) 0.5D (d) 1D (e) 2D (f) 4D. H is the hub height. The red lines indicate the range of the wind turbine rotor. Wind speed in (b) – (f) is normalized by U_{inflow} in (a). The error bars show the mean ± 1 standard deviation.

4. Conclusion

We performed wind turbine wake measurements using a Galion LiDAR at a flat terrain site in Japan and examined the influence of tip speed ratio on the wind turbine wake property. The obtained results are follows:

- Downstream recovery of the velocity deficit is more rapid at lower tip speed ratio.
- The twin-mountain shape of the profile brakes more slowly at higher tip speed ratio.
- The wind speed outside of the rotor range (at lower height) is accelerated in the near-wake, especially at high *TSR* region.

5. Future works

In this paper, we investigated the influence of tip speed ratio on the wind turbine wake property using a Galion LiDAR in order to store field test data for the development of a general wake model, including the influences of wind turbine operation. We achieved benchmark field test data at a flat terrain wind turbine site, which is the most basic site. We will conduct wake measurements using the LiDAR at complex terrain wind turbine sites and study the influence of terrain configuration on wake property.

We will also conduct wake measurements using the LiDAR operating yaw angle of a wind turbine and study the effect of yaw angle on wake property.

Acknowledgments

I acknowledge Japan Meteorological Corporation for their support in obtaining the LiDAR data measurements.

References

[1] L. J. Vermeer, J. N. Sørensen, and A. Crespo, "Wind turbine wake aerodynamics," *Prog. Aerosp. Sci.*, vol. 39, pp. 467–510, 2003.

[2] W. Tian, A. Ozbay, and H. Hu, "Effects of incoming surface wind conditions on the wake characteristics and dynamic wind loads acting on a wind turbine model," *Phys. Fluids*, vol. 26, no. 12, 2014.

[3] M. Bastankhah and F. Porté-Agel, "A wind-tunnel investigation of wind-turbine wakes in yawed conditions," *J. Phys. Conf. Ser.*, vol. 625, no. 1, 2015.

[4] Y. Kamada, J. Murata, T. Maeda, T. Ito, A. Okawa, S. Yonekura, and T. Kogaki, "Experimental Study on Wind Turbine Wake and Rotor Output in Wake with Various Turbulence Intensity," *Turbomachinery*, vol. 40, no. 2, pp. 97–103, 2012.

[5] T. Maeda, Y. Kinpara, and T. Kakinaga, "Wind Tunnel and Field Experiments on Wake Behind Horizontal Axial Wind Turbine," *Trans. JSME*, vol. 71, no. 701, pp. 162–170, 2005.

[6] B. Andresen, "Wake behind a wind turbine operating in yaw," *Nor. Univ. Sci. Technol.*, vol. Master of, 2013.

[7] P. Å. Krogstad and M. S. Adaramola, "Performance and near wake measurements of a model horizontal axis wind turbine," *Wind Energy*, vol. 15, pp. 743–756, 2012.

[8] G. More and D. Gallacher, "Lidar Measurements and Visualisation of Turbulence and Wake Decay Length," *EWEA*, 2014.

[9] G. V. Iungo, Y.-T. Wu, and F. Porté-Agel, "Field Measurements of Wind Turbine Wakes with Lidars," *J. Atmos. Ocean. Technol.*, vol. 30, no. 2, pp. 274–287, 2013.

[10] IEC, "IEC 61400 -12-2 Power performance of electricity-producing wind turbines based on nacelle anemometry," 2013.